Appendix

Methods

Subjects

Ninety-seven healthy volunteer datasets (n=77 HC_{PRE}; n=20 HC_{POST}) were available in our records. As shown in Suppl. Figure 1, three subjects were excluded for reported technical issues during data acquisition (n=2; HC_{PRE}) or the absence of COVID-19 antibody test (n=1; HC_{POST}). The remaining ninety-four scans were collected in seventy participants: fifty scanned once (39 HC_{PRE} ; 11 HC_{POST}), twenty-two scanned twice (18 HC_{PRE} ; 4 HC_{POST}). Of those, sixteen HC_{PRE} were scanned twice in the same scanner (Scanner 1), whilst the others were imaged in two different scanners. Two subjects were scanned before and after lockdown (one both times in Scanner 1; the other in two different scanners) and thus contributed to both the HC_{PRE} and HC_{POST} cohorts.

Overall, a final cohort of 72 data sets (57 HC_{PRE} ; 15 HC_{POST}) was obtained as follows. For those participants scanned twice in the same scanner, the scan acquired first was included in the main analyses, whereas the other scan was used for validation testing (see "Alternate dataset analysis" section). For the participants scanned twice in different scanners, we selected the scan that would support a balanced distribution across groups (i.e., for 4 $HC_{POST,}$ we used two datasets from Scanner 1 and two datasets from Scanner 2). Data collected with the other scanner were used for validation testing (see "Alternate dataset analysis" section).

PET data acquisition and processing

All participants were scanned for a time-period that included ~60-90 minutes post-injection (the framing window used in our PET analyses; see below). Due to protocol differences across the

various studies contributing data to this project, fifty-seven subjects (44 HC_{PRE}; 15 HC_{POST}) were injected on the scanner bed and continuously imaged for about 90 minutes, while a subset (15 HC_{PRE}) was injected outside the scanner and imaged ~40-90 minutes post-injection. Structural T1 images were acquired for the purpose of anatomical localization, spatial normalization of PET data, and generation of attenuation correction maps. For all subjects, thirty-minute static standardized uptake value (SUV) PET images were reconstructed from data acquired ~60-90 min after the injection of the tracer. PET data were scatter- and attenuation-corrected using a customed MR-based method developed at the Martinos Center For Biomedical Imaging. SUV maps were non-linearly transformed to Montreal Neurological Institute (MNI) space and smoothed with an 8mm full width at half-maximum Gaussian kernel to improve on signal to noise ratio (SNR).

^{1}H-MRS data acquisition and processing

^{1}H-MRS data were acquired using isotropic voxels positioned in the left thalamus with voxel sizes of 15 mm (Scanner 1) and 20 mm (Scanner 2). MRS data was analyzed using the software jMRUI v6.0. Spectra were phase-corrected and a Hankel Lanczos Singular Values Decomposition (HLSVD) filter was applied to remove the residual water signal. Signal-to-noise ratios (SNR) were determined by jMRUI QUEST in time-domain (maximum of FID/standard deviation of FID tail) and full-width-half maximum (FWHM) of unsuppressed water signals were measured using jMRUI-AMARES algorithm. Metabolite concentrations of the inflammatory marker mIns and, for reference, Creatine (Cr; a cellular energetic marker) and N-Acetyl Aspartate (NAA; a marker of neuronal integrity) were extracted. Metabolites were quantified with the QUEST algorithm (combined with 'Subtract' for background modelling) in jMRUI. QUEST metabolite basis set was quantum-mechanically simulated at 3T using a press protocol (TE=30ms, 1024 sample points, SW=1200Hz) in NMR Scope-B. Metabolite concentrations [mmol/l] are

reported relative to the water-unsuppressed spectra and concentrations were corrected for partial volume effects.

Behavioral data

To assess the clinical significance of our findings, all HC_{POST} participants were re-contacted between August and September 2021, with the invitation to complete (either via phone or email) a questionnaire assessing the impact of the pandemic on their mental and physical health. The questionnaire (Suppl. Table 5) consisted of ten questions taken from the more extensive "COVID-19 Impact on Health and Wellbeing Survey" (https://www.nlm.nih.gov/dr2/COVID_Impact_on_Health_Wellbeing_Eng.pdf), which were designed to assess the frequency of mood alterations during the pandemic (from "never" to "very often"). These questions where supplemented by 3 additional questions, assessing the presence and severity of mental fatigue, physical fatigue and dyscognition ("brain fog"), respectively (from "no" to "yes, substantially"). The mean of the first ten questions, and the scores of the last 3 questions were binarized using a median-split to categorize each participant into a "lower symptom burden" (e.g., "Never/almost never felt symptom X") or "higher symptom burden" subgroup (e.g., Symptom X experienced "sometimes" to "very often", or "slightly to "substantially"), for each symptom domain separately. Finally, the questionnaire also included ancillary items on the economic impact of the pandemic, and a question about having ever tested positive for COVID-19 at any point during the pandemic (not discussed further in this report). 11 out of 15 successfully completed the questionnaire.

Age-matched subanalysis

Given the significant difference in age across groups, we re-ran all group analyses using smaller subsets of HC_{PRE} ($HC_{PRE\text{-}Matched}$) who were better demographically matched to the HC_{POST} cohort. To this end, a subset of twenty-nine $HC_{PRE\text{-}Matched}$ was created from the main HC_{PRE} cohort, by removing all HC_{PRE} subjects with an age range 20-40 (n=28). This resulted in a non-statistical difference in age ($p=0.11$). The $HC_{PRE\text{-}Matched}$ group also showed no significant statistical difference, TSPO polymorphism, sex, injected dose, scanner and weight between the two groups (Supplementary Table 1).

The matched cohort analysis with ^{1}H-MRS was performed on the same subset of participants with ^{1}H-MRS data available, resulting in 9 $HC_{PRE\text{-}Matched}$ subjects, matched by age to the HC_{POST} cohort ($p=0.32$; Supplementary Table 2).

Alternate dataset analysis

PET and ^{1}H-MRS analyses were repeated by replacing, for subjects scanned twice, the primary dataset as the secondary (ie., as described above). Alternate scans were used for 18 HC_{PRE} and 4HC_{POST} subjects in the PET analyses, and for 1 HC_{PRE} and 2 HC_{POST} in the ^{1}H-MRS analysis.

Unvaccinated-only analysis

PET and ^{1}H-MRS analyses were repeated by comparing all HC_{PRE} subjects included in the main analyses with only the subset of HC_{POST} subjects who, at the time of the scan, had not (yet) received any of the available vaccines against the SARS-CoV-2 virus: 9 for the PET analyses and 57 for the^{1}H-MRS analyses.

Pre-lockdown "time stability" analyses

In order to understand how the increase in neuroinflammatory signals observed post-lockdown compared to natural variations due to passing of time, we performed both between- and within-subject "time stability tests" using pre-lockdown [^{11}C]PBR28 data. For the between-subject tests, the HC_{PRE} group was subdivided into two subgroups, which were then compared against each other. The first subgroup ($HC_{PRE\text{-}2012/2015}$) included data from 2012 to 2015 (N=14, sex=9M; 5F, genotype=10HAB; 4MAB, Scanner 1=14; Scanner 2=0, age=43.8±12.46). The second ($HC_{PRE\text{-}2016/2020}$) included data collected from 2016 until lockdown (N=43, sex=21M; 22F, genotype=23HAB; 20MAB, Scanner 1=20; Scanner 2=13, age=41.45±15.8). The two groups were identified 1) based on the clustering of the scan dates (reflecting the scanning gap in 2015-2016; see Results), and 2) to approximate the difference in sample size, and scanner / genotype proportions observed in the main analysis comparing HC_{PRE} and HC_{POST}. The PET signal from $HC_{PRE\text{-}2012/2015}$ and $HC_{PRE\text{-}2016/2020}$ were compared using ROI analyses, extracting the mean from the same subclusters identified as statistically different between HC_{PRE} and HC_{POST} in the main analyses (see Results), Bonferroni-corrected for number of regions. These pre-lockdown groups were further compared using non-parametric whole-brain voxel-wise permutation inference. Both analyses included the same regressors as for the main analysis (i.e., age, TSPO polymorphism, scanner).

For the within-subject tests, a subset of 15 subjects from HC_{PRE}, with available re-scans ($HC_{PRE\text{-}scan1}$ and $HC_{PRE\text{-}scan2}$) close in time (2 to 8 months) from the same scanner (Scanner 1), were compared against each other to assess within-subject variability. In this case, paired tests were used in both ROI and voxel-wise analyses.

PET kinetic analysis

A subset of twenty-nine subjects (20 HC_{PRE} and 9 HC_{POST}) received a radial artery catheter at the time of the scan, and blood samples were collected at ~5, 10, 20, 30, 50, 70 and 90 minutes post radiotracer injection. Uncorrected plasma curves were obtained from raw blood samples using linear fitting. In fifteen subjects, arterial blood processing was performed using a HyperSep C18 solid extraction cartridge to separation of radio-metabolites; in nine subjects, High Performance Liquid Chromatography (HPLC) for separation of radio-metabolites from parent radiotracer was used instead. Hill-fitted parent fractions were applied to the raw data and a radio-metabolite-corrected arterial input function (AIF) was obtained for each subject. Previous cross-validation confirmed reliability of both pipelines allowing us to combine both datasets to increase statistical power of our study. Of all the available blood data, 4 HC_{PRE} and 1 HC_{POST} blood-data were not completely processed due technical difficulties during sample collection; thus, those subjects were excluded from any kinetic analysis, resulting in a final cohort of 16 HC_{PRE} and 8 HC_{POST}. Dynamic 0-90 SUV PET images were reconstructed in twenty-eight frames of increasing duration. Then, AIFs and 4D PET SUV images were used as the input for a Logan plot analysis: the blood curve was down-sampled to PET space and the curves of tissue region-of-interest and arterial plasma were transformed and combined into a single curve. It was assumed they approached linearity after a time $t^* = 15min$; thus, the linear regression was computed on the last 11 frames. The slope of the fitted line represents the distribution volume (Vt); the DVRs were extracted in the parcellates of the cluster significant in the main group analyses, using the same normalization region as for SUVR calculation. Group differences were assessed using the same model as for the SUVR analysis.

Imaging Transcriptomics

Transcriptomic data. Regional microarray expression data were obtained from six post-mortem brains as part of the AHBA (http://human.brain-map.org/) (ages 24–57 years). We used the *abagen* toolbox (https://github.com/netneurolab/abagen) to process and map the transcriptomic data onto the 83 parcellated brain regions from the Desikan-Killiany (DK) atlas. Briefly, genetic probes were reannotated using information provided by Arnatkeviciute et al., 2019 [1] instead of the default probe information from the AHBA dataset, hence discarding probes that cannot be reliably matched to genes. Following previously published guidelines for probe-to-gene mappings and intensity-based filtering [1], the reannotated probes were filtered based on their intensity relative to background noise level (i.e., probes with intensity lower than the background in ≥50% of samples were discarded). A single probe with the highest differential stability (highest pooled correlation across donors) was selected to represent each gene [2]. This procedure retained 15,633 probes, each representing a unique gene. Next, tissue samples were assigned to brain regions using their corrected MNI coordinates (https://github.com/chrisfilo/alleninf) by finding the nearest region within a radius of 2 mm. To reduce the potential for misassignment, sample-to-region matching was constrained by hemisphere and cortical/subcortical divisions. If a brain region was not assigned to any sample based on the above procedure, the sample closest to the centroid of that region was selected to ensure that all brain regions were assigned a value. Samples assigned to the same brain region were averaged separately for each donor. Gene expression values were then normalized separately for each donor across regions using a robust sigmoid function and rescaled to the unit interval. We applied this procedure for cortical and subcortical regions separately, as suggested by Arnatkeviciute et al., 2019 [1]. Scaled expression profiles were finally averaged across donors, resulting in a single matrix with rows corresponding to brain regions and columns

corresponding to the retained 15,633 genes. As a further robustness test, we conducted leave-one-donor out sensitivity analyses to generate six expression maps containing gene expression data from all donors, one at a time. The principal components of these six expression maps were highly correlated (average Pearson's correlation of 0.993), supporting the notion that our final gene expression maps, averaged by region across all six donors, is unlikely to be biased by data from a specific donor. Since the AHBA only includes data for the right hemisphere for two subjects, we only considered the 41 regions of left hemisphere regions (34 cortical plus 7 subcortical regions) for the following analyses.

Partial least square regression. Partial least square regression uses the gene expression measurements (the predictor – or independent – variables) to predict regional variation in neuroimaging features (the response – or dependent – variables). This approach allows us to rank all genes by their multivariate spatial alignment with the regional distribution of each neuroimaging feature, while accounting for inherent collinearity in the predictor variables due to gene co-expression. The first PLS component (PLS_1) is the linear combination of the weighted gene expression scores that have a brain expression map that covaries the most with the neuroimaging map. As the components are calculated to explain the maximum covariance between dependent and independent variables, the first component does not necessarily need to explain the maximum variance in the dependent variable. Of note, as the number of PLS components calculated increases, the amount of variance explained by each of them progressively decreases. Here, we examined models across a range of components (between 1 and 15) and evaluated the relative variance explained by each component against 1,000 null models, where we preserved the spatial autocorrelation of the data (see the section 'spatial permutation test' for more details). We then moved to further analyses only the PLS component explaining the largest amount of variance,

which was the first component (PLS_1). The error in estimating each gene's PLS_1 weight was assessed by bootstrapping (resampling with replacement of the 41 brain regions), and the ratio of the weight of each gene to its bootstrap standard error was used to calculate the *Z* scores and, hence, rank the genes according to their contribution to PLS_1 [3]. Genes with large positive PLS_1 weights correspond to genes that have higher than average expression in regions where post-lockdown [^{11}C]PBR28 signal increased, and lower than average expression in regions where [^{11}C]PBR28 signal changed the least. Mid-rank PLS weights showed expression gradients that are weakly related to the pattern of regional distribution of [^{11}C]PBR28 signal changes. On the other hand, genes with large negative PLS weights correspond to genes that have higher than average expression in regions where [^{11}C]PBR28 signal changed the least, and lower than average expression in regions with the largest increases in [^{11}C]PBR28 signal. Since in our analyses we were mostly interested in genes that track the magnitude of increases in [^{11}C]PBR28 signal, we focused on genes with positive PLS weights (even if we also present the results for genes with negative PLS weights for completeness).

Spatial permutation test (spin test): We assessed the significance of correlation between the [^{11}C]PBR28 signal changes and PLS_1 using spatial permutation testing (spin test) to account for the inherent spatial autocorrelation of the imaging data, as implemented in previous studies [4]. This approach consists in comparing the empirical correlation amongst two spatial maps to a set of null correlations, generated by randomly rotating the spherical projection of one of the two spatial maps before projecting it back onto the brain parcel. Importantly, the rotated projection preserves the spatial contiguity of the empirical maps, as well as the hemispheric symmetry. Past studies using the spin test have focused on comparisons between brain maps including only cortical regions. However, subcortical regions were also of interest in this study. Since subcortical regions

cannot be projected onto the inflated spherical pial surface, we incorporated the subcortex into our null models by shuffling the seven subcortical regions with respect to one another, whereas the cortical regions were shuffled using the spin test.

Gene set enrichment analyses. We used the PLS_1-ordered list of genes, ranked by the respective weights, to perform gene set enrichment analyses (GSEA) for biological pathways (gene ontology) and genes expressed in different brain cell types (see section on single-cell transcriptomic data below). We implemented these analyses using the GSEA method of interest of the Web-based gene set analysis toolkit (*WebGestalt*) [5]. In contrast to other over-representation methods, GSEA does not require the definition of an arbitrary threshold to isolate the most highly associated genes with a certain phenotype. It calculates an enrichment ratio (ER) that represents the degree to which the genes in the set are over-represented at either the top (positive ER) or bottom (negative ER) of the list, based on a Kolmogorov-Smirnov-like statistic. Then, it estimates the statistical significance of the ER using permutations to produce a null distribution for the ER (we used 1,000 permutations). The significance is determined by comparison to the null distribution. Finally, it adjusts for multiple hypothesis testing when several gene sets are being analysed at one time. The enrichment scores for each set are normalized (NER) to account for the number of genes in each gene set and a false discovery rate correction is applied.

Single-cell transcriptomic data. We compiled data from five different single-cell studies using *post-mortem* cortical samples in human postnatal subjects to avoid any bias based on acquisition methodology or analysis or thresholding [6,7]. To obtain gene sets for each cell type, categorical determinations were based on each individual study, as per the respective methods and analysis choices in the original paper. All cell-type gene sets were available as part of the respective papers. We generated a single omnibus gene list for each cell type by merging the study-

specific gene lists, and then filtered it to retain only genes sampled in the AHBA. Two studies did not subset neurons into excitatory and inhibitory [7,8], and thus those gene sets were excluded from the cell-class assignment. Additionally, only one study included the annotation of the "Per" (pericyte) type, and thus we did not consider that cell type [6]. This approach has already been validated elsewhere [9].

Tables and figures

		$HC_{PRE\text{-}Matched}$	HC_{POST}	p
N		29	15	
Sex	Male Female	19 (65.5) 10 (35.5)	12 (80) 3 (20)	0.31
Age [y]		55.72(9.49)	60.73(10.7)	0.11
TSPO genotype	HAB MAB	16(55.1) 13(44.9)	7 (46.6) 8 (53.4)	0.59
Scanner	Scanner 1 Scanner 2	21(72.4) 8(27.6)	9 (60) 6 (40)	0.40
Weight [kg]		73.86(16.94)	78.04(19.7)	0.46
Inj. Dose [mCi]		13.26(1.66)	13.86(1.69)	0.26

Supplementary Table 1. Demographics from the matched [^{11}C]PBR28 PET cohorts ($HC_{POST\text{-}MATCHED}$ vs HC_{PRE}). Categorical variables are summarized as frequencies (proportions) and continuous variables are summarized as mean (standard deviation). HAB=high affinity binders; MAB=mixed affinity binders; mCi=millicuries.

		$HC_{PRE\text{-}Matched}$	HC_{POST}	p
N		9	11	
Sex	Male Female	6 (66.7) 3 (33.3)	8 (72.7) 3 (27.3)	0.76
Age [y]		55.25(7.95)	60.36(12.2)	0.32
Scanner	Scanner 1 Scanner 2	2(22.2) 7(77.8)	6 (54.5) 5 (45.5)	0.14
Weight [kg]		78.03(13.76)	76.73(22.61)	0.88

Supplementary Table 2. **Demographics from the matched ^{1}H-MRS cohorts ($HC_{POST\text{-}MATCHED}$ vs HC_{PRE}).** Categorical variables are summarized as frequencies (proportions) and continuous variables are summarized as mean (standard deviation).

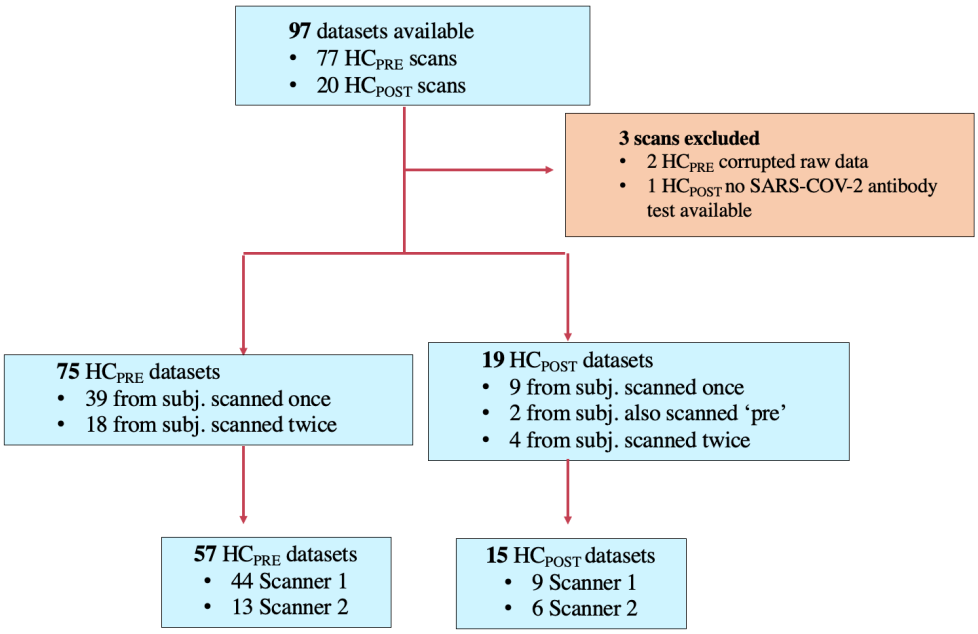

Supplementary Figure 1. Flow diagram illustrating dataset inclusion in the study. In subjects scanned twice, one of the two scans was used for the main analyses (see Appendix), whereas the other was used for validation. Two subjects were scanned before and after lockdown (one both times in Scanner 1; the other in two different scanners) and thus contributed to both the HC_{PRE} and HC_{POST} cohorts. The subject scanned both times in Scanner 1 was used to assess within-subject changes in PET signal.

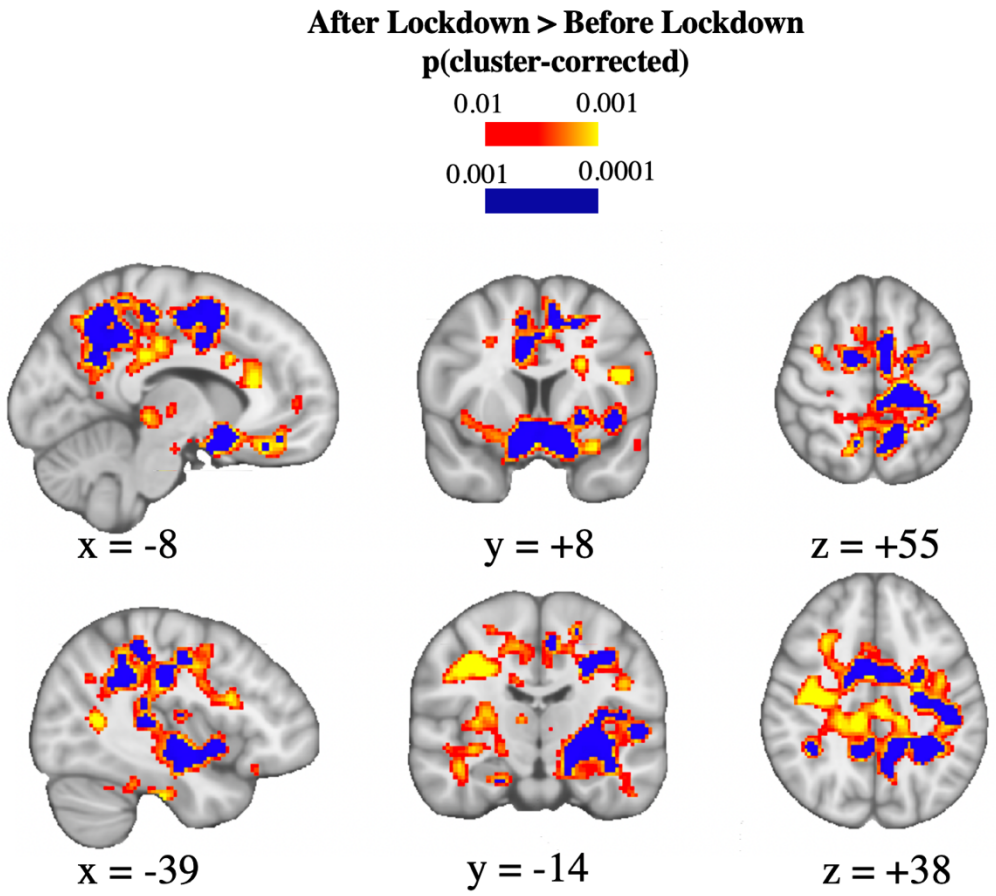

Supplementary Figure 2. Significant voxelwise group differences (HC_{POST}>HC_{PRE}) at a more conservative threshold. Cluster-forming threshold of p=0.001 with cluster-size threshold of p = 0.05 (blue color scale), overlaid on the results of the main group differences (see Methods; yellow/red color scale) (FSL randomise; 5000 permutations).

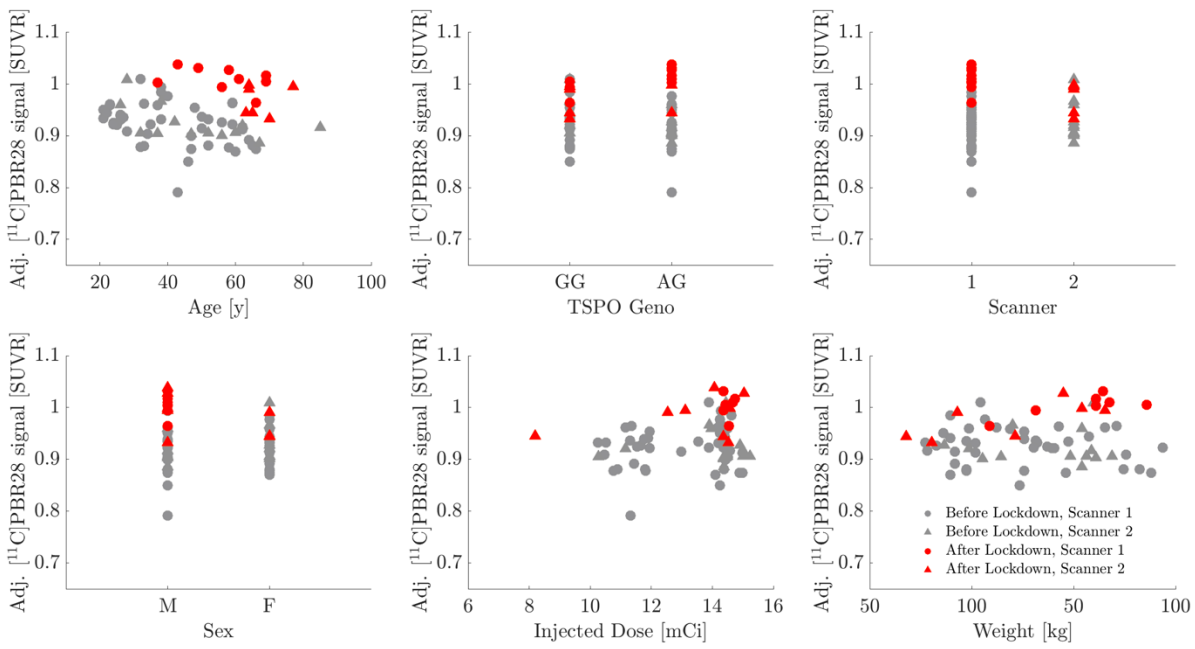

Supplementary Figure 3. Mean [^{11}C]PR28 PET signal displayed across ages, genotypes, scanners, sex, injected dose and weight. Mean SUVR extracted from the cluster significant in voxel-wise group comparisons, using a cluster-forming threshold of p=0.001. The signal appears consistently higher in HC_{POST} than HC_{PRE}, irrespective of these factors.

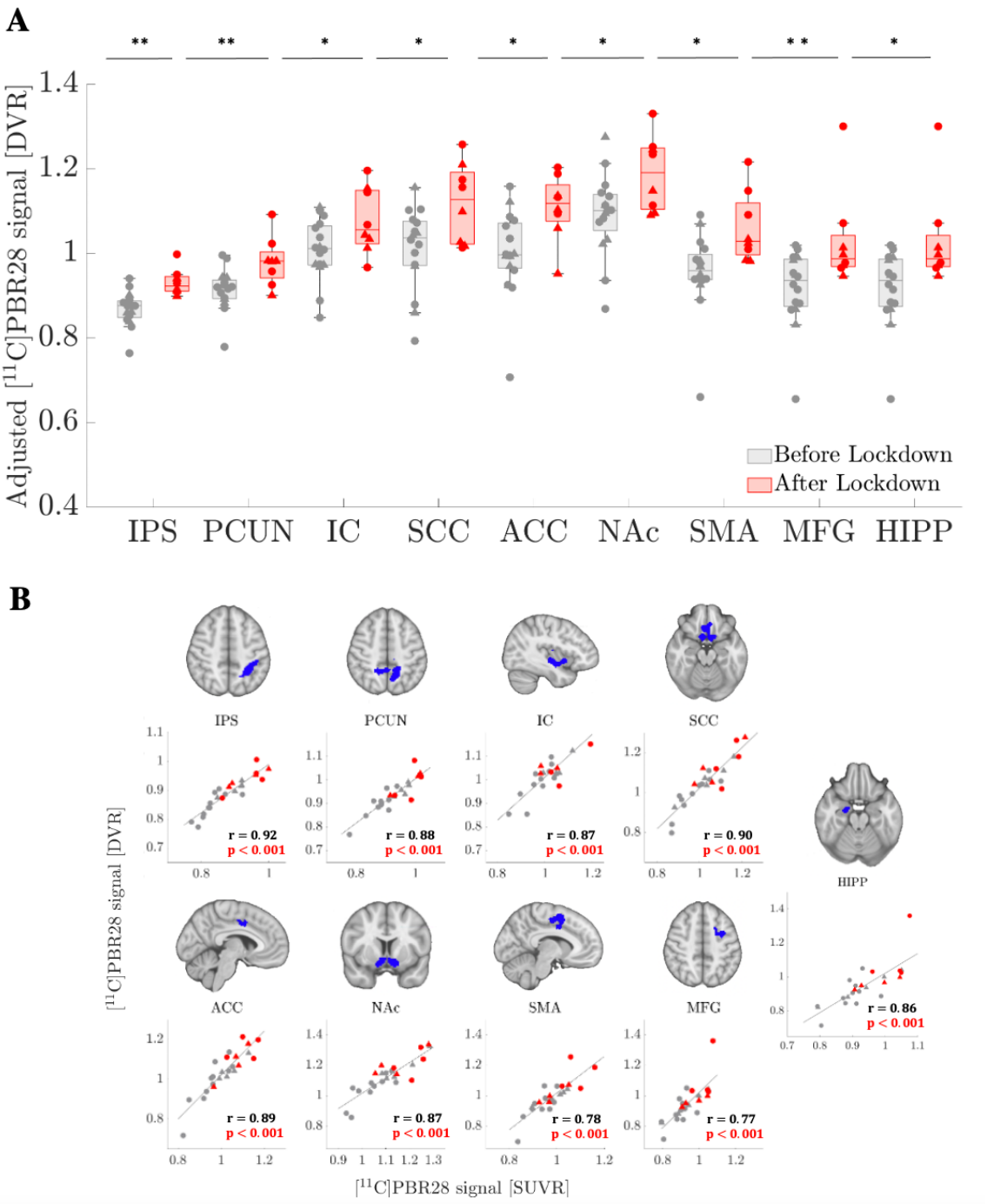

Supplementary Figure 4. Comparison of SUVR and DVR metrics. (A) Group comparison of before lockdown (HC_{PRE}) and after lockdown (HC_{POST}) subjects with available arterial-line data, adjusting for scanner age and genotype. (B) [^{11}C]PBR28 standardized volume ratio (SUVR) uptake signal correlations with distribution volume ratio (DVR). See Figure 2 caption for abbreviations.

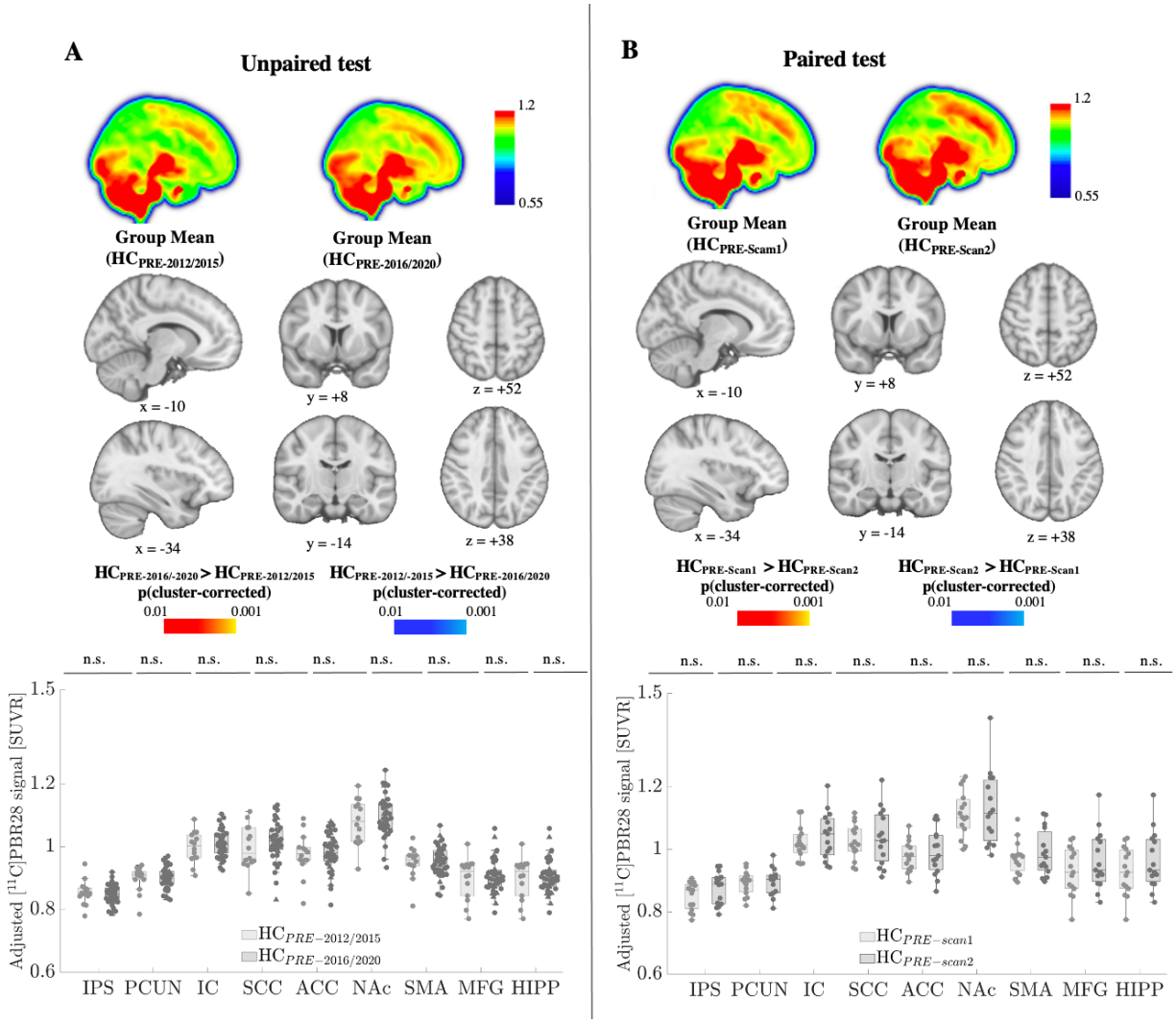

Supplementary Figure 5. Pre-lockdown [^{11}C]PBR28 PET signal "time stability" tests. Unpaired (A) and paired (B) tests conducted on two subgroups from the main 'pre-lockdown' cohort, via voxel-wise group contrast analysis (using the same statistical model as in the main analysis). Mean images from each subgroup are displayed as maximum intensity projection (MIP). Error bars represent the 25th to 75th inter-quartile range. Triangles denote data from Scanner 1 and circles denote data from Scanner 2. See Figure 2 captions for abbreviations.

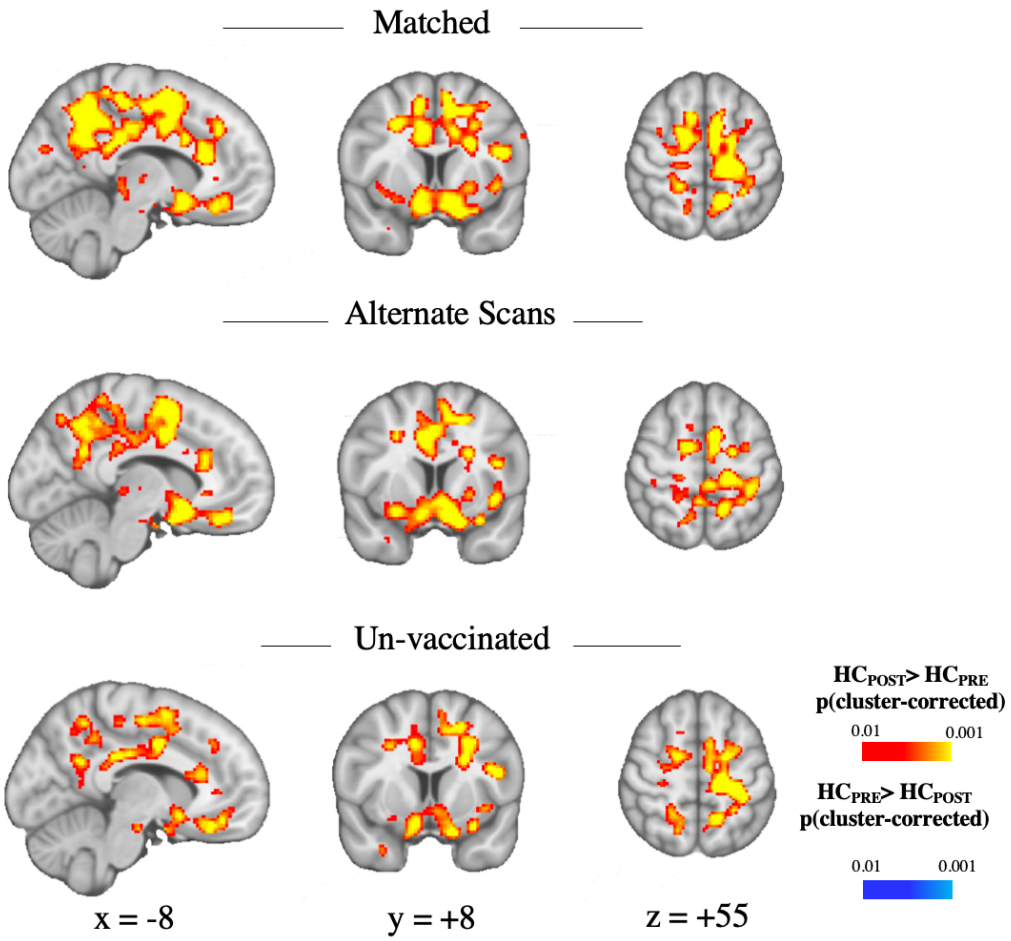

Supplementary Figure 6. [^{11}C]PBR28 PET sensitivity analyses. Areas of elevated post-lockdown PET [^{11}C]PBR28 SUVR signal in (A) "age-matched" (B) "alternate dataset" and (C) "unvaccinated-only" subanalyses.

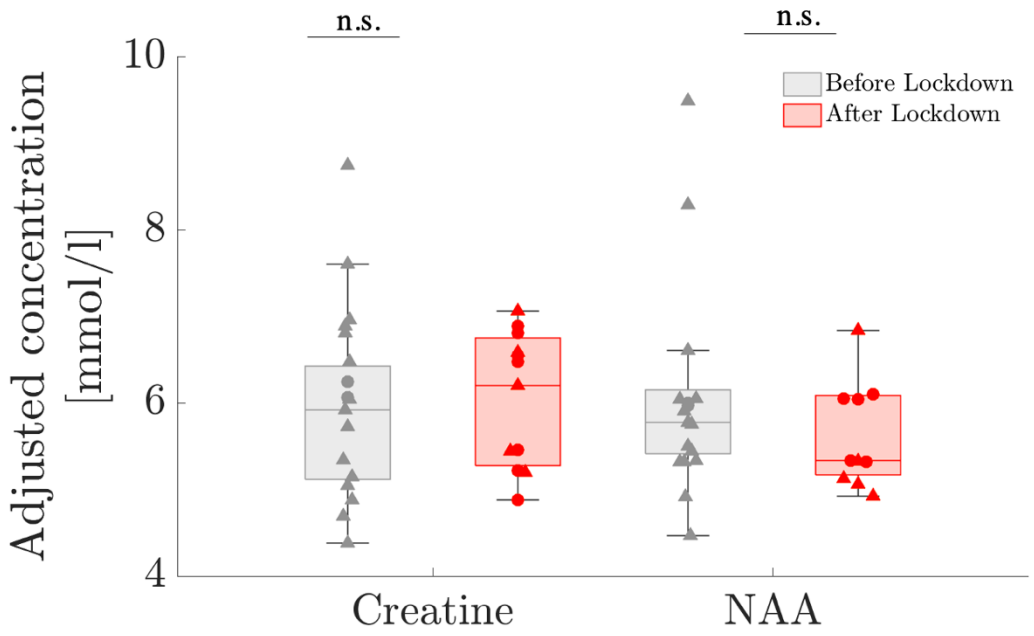

Supplementary Figure 7. Group comparison for reference ^{1}H-MRS metabolites. Creatine (a cellular energetic marker) and N-Acetyl Aspartate (NAA; a marker of neuronal integrity), acquired in the left thalamus. Error bars denote 25th to 75th inter-quartile range. Triangles denote data from Scanner 1 and circles denote data from Scanner 2.

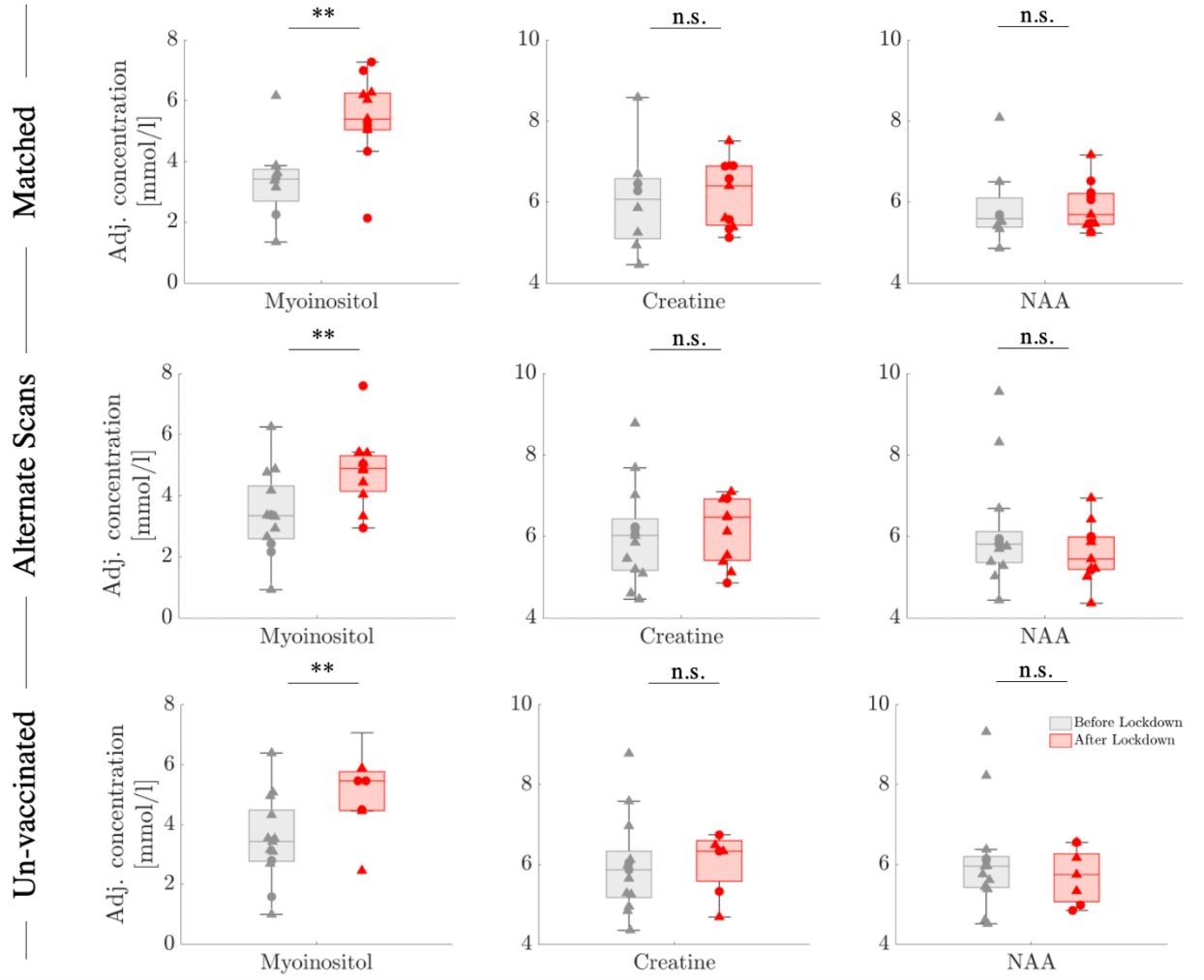

Supplementary Figure 8. ^{1}H-MRS sensitivity analyses. (A) "age-matched", (B) "alternate dataset" and (C) "unvaccinated-only" subanalyses. Boxes represent the 25th to 75th inter-quartile range. Triangles denote data from Scanner 1 and circles denote data from Scanner 2. NAA=N-Acetyl Aspartate.

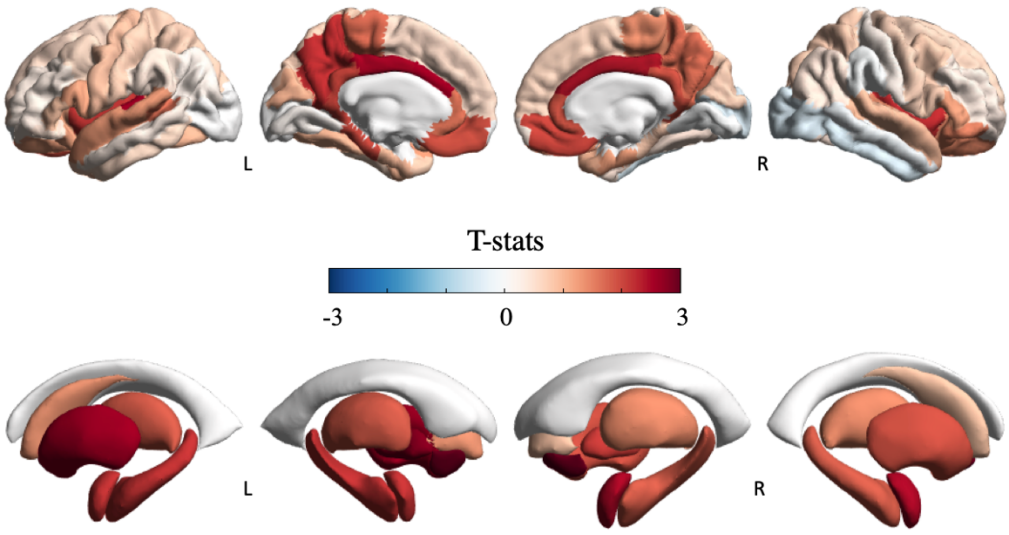

Supplementary Figure 9. Visualization of pre/post-lockdown [^{11}C]PBR28 changes in the Desikan-Killiany atlas. Regional distribution of the T-statistics quantifying changes in [^{11}C]PBR28 signal in HC_{POST} subjects compared to HC_{PRE} subjects in each of the 82 cortical (upper row) and subcortical (lower row) regions of the Desikan-Killiani atlas; brainstem not depicted.

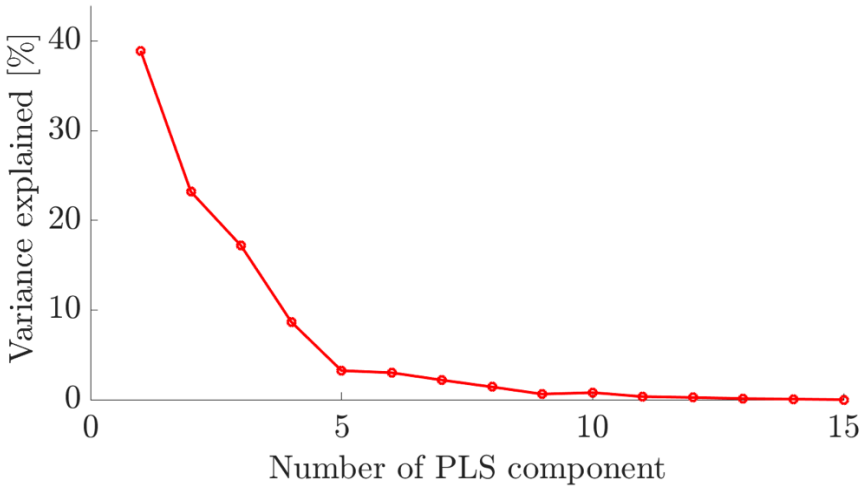

Supplementary Figure 10. PLS and percentage of variance explained. Percentage of variance explained in [^{11}C]PBR28 changes (HC_{POST} minus HC_{PRE}) by each independent component of the partial least square regression models

Cell-type	NER	p_{FDR}
Excitatory Neurons	-1.83	<0.001
Inhibitory Neurons	-1.41	0.003
Endothelial cells	-1.07	0.480
Oligodendrocytes	2.04	<0.001
Oligodendrocyte precursor cells	2.19	<0.001
Microglia	2.33	<0.001
Astrocytes	3.39	<0.001

Supplementary Table 3. Brain cell-type gene set enrichment analysis. Abbreviations: NER – Normalized Enrichment Ratio; FDR – False-Discovery Rate.

Gene set	Description	NER	p_{FDR}
GO:0070972	protein localization to endoplasmic reticulum	3.228	<0.001
GO:0006413	translational initiation	2.804	<0.001
GO:0042116	macrophage activation	2.537	<0.001
GO:0002181	cytoplasmic translation	2.349	0.001
GO:0006401	RNA catabolic process	2.413	0.001
GO:0090150	establishment of protein localization to membrane	2.232	0.001
GO:0002269	leukocyte activation involved in inflammatory response	2.192	0.002
GO:0006968	cellular defense response	2.199	0.002
GO:0050866	negative regulation of cell activation	2.124	0.004
GO:0070661	leukocyte proliferation	2.084	0.005
GO:0035587	purinergic receptor signaling pathway	2.042	0.006
GO:0006605	protein targeting	2.043	0.007
GO:0150076	neuroinflammatory response	1.985	0.010
GO:0140053	mitochondrial gene expression	-2.013	0.010
GO:0031128	developmental induction	1.987	0.010
GO:0042063	gliogenesis	1.940	0.014
GO:0045576	mast cell activation	1.930	0.015
GO:0002694	regulation of leukocyte activation	1.920	0.015
GO:0035329	hippo signaling	1.879	0.021
GO:0033627	cell adhesion mediated by integrin	1.814	0.029
GO:0006959	humoral immune response	1.817	0.029
GO:0032103	positive regulation of response to external stimulus	1.805	0.029
GO:0042110	T cell activation	1.826	0.029
GO:0032623	interleukin-2 production	1.837	0.030
GO:0002448	mast cell mediated immunity	1.833	0.030
GO:0034109	homotypic cell-cell adhesion	1.799	0.030
GO:0002437	inflammatory response to antigenic stimulus	1.790	0.030
GO:0050867	positive regulation of cell activation	1.826	0.030
GO:0002697	regulation of immune effector process	1.791	0.031
GO:0032602	chemokine production	1.782	0.031
GO:0002237	response to molecule of bacterial origin	1.770	0.031
GO:0001773	myeloid dendritic cell activation	1.773	0.031
GO:0051339	regulation of lyase activity	1.765	0.032
GO:0070371	ERK1 and ERK2 cascade	1.773	0.032
GO:0000959	mitochondrial RNA metabolic process	-1.896	0.038
GO:0032104	regulation of response to extracellular stimulus	1.740	0.038
GO:0043583	ear development	1.724	0.043
GO:0032418	lysosome localization	1.701	0.044
GO:0002526	acute inflammatory response	1.704	0.044

GO:0023019	signal transduction involved in regulation of gene expression	1.675	0.045
GO:0060191	regulation of lipase activity	1.705	0.045
GO:0060326	cell chemotaxis	1.695	0.045
GO:0031532	actin cytoskeleton reorganization	1.682	0.045
GO:0031279	regulation of cyclase activity	1.685	0.046
GO:0034367	protein-containing complex remodeling	1.679	0.046
GO:0023058	adaptation of signaling pathway	1.691	0.046
GO:0050663	cytokine secretion	1.706	0.046
GO:0050727	regulation of inflammatory response	1.675	0.046
GO:0007159	leukocyte cell-cell adhesion	1.668	0.046
GO:0032612	interleukin-1 production	1.710	0.046
GO:0098727	maintenance of cell number	1.685	0.046
GO:0061614	pri-miRNA transcription by RNA polymerase II	1.706	0.047
GO:0022407	regulation of cell-cell adhesion	1.664	0.047

Supplementary Table 4. Gene set enrichment analysis. Gene Ontology Biological Pathway.

Abbreviations: NER – Normalized Enrichment Ratio; FDR – False-Discovery Rate.

	Between when the lockdown started around March 2020 and when you were scanned on [date] how often have you:
Q1	Been upset because of something that happened unexpectedly?
Q2	Felt that you were unable to control the important things in your life?
Q3	Felt nervous and stressed?
Q4	Felt confident in your ability to handle your personal problems?
Q5	Felt that things were going your way?
Q6	Found that you could not cope with all the things you had to do?
Q7	Been able to control irritations in your life?
Q8	Felt that you were on top of things?
Q9	Been angered because of things that happened that were outside of your control?
Q10	Felt difficulties were piling up so high that you could not overcome them?
Q11	Did you experience higher mental fatigue than before?
Q12	Did you experience higher physical fatigue than before?
Q13	Did you experience any difficulty concentrating or “brain fog?”

Supplementary Table 5. **Questionnaire on the impact of the COVID-19 pandemic on mental and physical health**. Q1-Q10 were answered on 1-5 scale (1=“Never”; 5=”Very often”); scoring for questions 4-5, 7-8, was reversed prior to averaging. Q11-Q13 were answered on a 1-4 scale (1=“No”; 4=”Yes, substantially”).

Bibliography

1. Arnatkeviciute A, Fulcher BD, Fornito A. A practical guide to linking brain-wide gene expression and neuroimaging data. *Neuroimage* 2019; **189**: 353-67.
2. Hawrylycz M, Miller JA, Menon V, et al. Canonical genetic signatures of the adult human brain. *Nat Neurosci* 2015; **18**(12): 1832-44.
3. Whitaker KJ, Vértes PE, Romero-Garcia R, et al. Adolescence is associated with genomically patterned consolidation of the hubs of the human brain connectome. *Proceedings of the National Academy of Sciences of the United States of America* 2016; **113**(32): 9105-10.
4. Alexander-Bloch A, Giedd JN, Bullmore E. Imaging structural co-variance between human brain regions. *Nat Rev Neurosci* 2013; **14**(5): 322-36.
5. Zhang B, Kirov S, Snoddy J. WebGestalt: an integrated system for exploring gene sets in various biological contexts. *Nucleic Acids Res* 2005; **33**(Web Server issue): W741-8.
6. Lake BB, Chen S, Sos BC, et al. Integrative single-cell analysis of transcriptional and epigenetic states in the human adult brain. *Nat Biotechnol* 2018; **36**(1): 70-80.
7. Zhang Y, Sloan SA, Clarke LE, et al. Purification and Characterization of Progenitor and Mature Human Astrocytes Reveals Transcriptional and Functional Differences with Mouse. *Neuron* 2016; **89**(1): 37-53.
8. Darmanis S, Sloan SA, Zhang Y, et al. A survey of human brain transcriptome diversity at the single cell level. *Proc Natl Acad Sci U S A* 2015; **112**(23): 7285-90.
9. Seidlitz J, Nadig A, Liu S, et al. Transcriptomic and cellular decoding of regional brain vulnerability to neurogenetic disorders. *Nat Commun* 2020; **11**(1): 3358.